Flow and Heat Transfer over Rough Surfaces:
Usefulness of 2-D Roughness-Resolved Simulations

S. Yoon[1], S. Na[1], Z.J. Wang[2], J. P. Bons[3], and T.I-P. Shih[4]

[1,2,4]Department of Aerospace Engineering, Iowa State University, Ames, Iowa 50011
[3]Department of Mechanical Engineering, Brigham Young University, Provo, UT 84602

Computations, based on the Fluent-UNS code with second-order upwind differencing and the realizable k-ε model, were performed to study the flow and heat transfer over two-dimensional (2-D) roughness geometries that resolve the details of the jagged surface. Parameters studied include height of approaching boundary layer to average roughness height (3.0 to 30) for the same rough surface and eight different rough surfaces with the same approaching boundary layer in which the average roughness height, rms, skewness, and kurtosis of the roughness vary in the ranges of 0.748 to 1.480, 0.991 to 1.709, -1.509 to 0.356, and 1.927 to 3.136, respectively. Results are presented for the contributions to the friction coefficient from shear and from pressure – locally and averaged over the entire rough surface. Also presented are the computed flow fields and the averaged Stanton numbers for all rough surfaces studied. Results obtained by the 2-D roughness-resolved simulations were compared with experimental data.

1. INTRODUCTION

Gas-turbine components operate in very harsh environments. All surfaces such as blades, vanes, endwalls, and hubs that come in contact with the combustor's hot gases invariably become rough with service.[1-3] The degree and the nature of the roughness due to mechanisms such as erosion, fuel deposition, corrosion, and spallation of thermal-barrier coatings depend on the environment from which the air is ingested, the engine operating conditions, the effectiveness of cooling management in maintaining material temperatures within acceptable limits, and the duration of service. Some examples of roughness that can form on turbine material surfaces are shown in Fig. 1. The roughness that forms on the surfaces is a sign of material degradation. In addition, it has been shown that the roughness significantly increases skin friction and surface heat transfer.[4-8] Increase in skin friction adversely affects aerodynamic performance, and increase in surface heat transfer raises material temperature, which hastens further material degradation.

The significant adverse effects created by surface roughness on skin friction and surface heat transfer have lead many investigators to study this problem. Previous efforts on modeling the effects of roughness on skin friction and surface heat transfer have met with mixed results. In particular, the concept of equivalent sandgrain roughness for skin friction coupled with Reynolds analogy for surface heat transfer – pioneered by Prandtl & Schlichting[9] and Schlichting[10] based on the experimental data of Nikuradse[11] – cannot adapt to the range of surface conditions typical of turbines. This is true despite the advances made by Coleman, et al.,[12] Sigal & Danberg,[13] Boyle,[14] Guo, et al.,[15] Bons,[16] Bergstrom, et al.,[17] and others.[18] Models that account for more of the details of the flow about the roughness geometry such as the discrete element method[19] have shown greater promise, but so far have not been successful in modeling flow and heat transfer of roughness surfaces caused by erosion, pitting, and spallation. The mixed result obtained by these earlier models is expected. Rough surfaces with highly irregular and distinctive valleys and peaks can introduce considerable vorticity and unsteadiness into the flow so that simple boundary-layer theory, van Driest type of damping, and Reynolds analogy may not apply.

First-principle simulations – that resolve every detail of the roughness geometry and the flow phenomena that they induce – offer an opportunity to obtain the understanding needed to construct engineering models for design and analysis. Wang, et al.[20] made such an attempt, where detach-eddy simulation (DES) and Reynolds-

---

[1] Graduate Student.
[2] Associate Professor. Associate Fellow AIAA.
[3] Associate Professor. Member AIAA.
[4] Professor and Chairperson. Associate Fellow AIAA.

Averaged-Navier-Stokes (RANS) simulations based on the Spalart-Almaras turbulence model[21] were used to simulate flow and heat transfer over a turbine rough surface, measured by Bon, et al.[3] However, DES, which uses RANS simulations in the near-wall region and large-eddy simulation (LES) further away from the walls, is computationally intensive. There are two reasons for this. The first is that LES demands transient three-dimensional (3-D) analysis that must resolve all relevant time and spatial scales of the turbulence. The second is that an enormous amount of grid points or cells are also needed to resolve the details of the roughness geometry. Thus, even with RANS in the near-wall region, the number of grid points needed to resolve the multi-scaled roughness geometry is significant. In addition, since many simulations are needed to understand the effects of roughness parameters, DES and LES are clearly not feasible. In fact, even 3-D RANS simulations of rough surfaces was found to be a major challenge in terms of both CPU time and memory requirements because of the enormous number of grid points needed to resolve the detail geometry of the roughness.

Since 3-D roughness-resolved simulations are a challenge, the objective of this study is to examine the usefulness and the roles of two-dimensional (2-D) RANS simulations in revealing the flow and heat transfer of 3-D rough surfaces. The organization of the remainder of this paper is as follows: First, we describe the rough surface problems studied. Next, we summarize the grid, the grid sensitivity study, and validation of this study for a flat plate problem with experimental data. Then, we present the results of our 2-D roughness-resolved simulations and comparisons with experiments.

2. PROBLEM DESCRIPTION

A schematic diagram of the 2-D rough-surface problem studied is shown in Fig. 2. For this problem, the wall is made up of three sections: an inviscid flat-plate section, a viscous flat-plate section, and the viscous rough wall section. The purpose of the inviscid wall section (L_1 = 0.5m) is to ensure the leading-edge of the boundary-later is resolved correctly. The purpose of the viscous flat-plate section (L = 0.1, 0.2, 0.5, 1, 2, and 3 m) is to control the thickness of the boundary-layer approaching the rough surface. The third section is the 2-D rough surface, the details of which are given later in this section. The origin of the coordinate system is placed at the beginning of the rough surface.

For this problem, the computational domain is taken to be the region bounded by the solid lines shown in Fig. 2. As can be seen, symmetry or an inviscid wall is placed at 0.3 m away from the rough wall. Since 0.3 m is much larger than the roughness height and displacement thickness, this domain approximates well uniform flow past a flat plate.

The flow conditions for this problem are as follows. At the inflow boundary, the velocity and temperature profiles are uniform at T_∞ of 300 K and velocity U_∞ of 10 m/s along x. The walls are adiabatic on the inviscid and viscous flat-plate sections. For the rough section, the wall temperature is 400K. The back pressure at the end of the plates was set at 1 atm.

Now, we describe the rough-surface section. Figure 3 shows the 3-D rough surface studied by Bons, et al.[3,8] For this 3-D surface, the statistics – R_a (average roughness height), R_q (rms roughness height) R_{sk} (skweness of roughness), and K_u (kurtosis) – are as follows:

$$R_a = \frac{1}{N} \sum_{i=1}^{N} \left| y_{average} - y_i \right| = 1.17\,mm \qquad (1)$$

$$R_q = \sqrt{\frac{1}{N} \sum_{i=1}^{N} \left(y_{average} - y_i \right)^2} = 1.44\,mm \qquad (2)$$

$$R_{sk} = \left\{ \frac{1}{N} \sum_{i=1}^{N} y_i^3 \right\} \frac{1}{R_q^3} = 0.11 \qquad (3)$$

$$K_u = \left\{ \frac{1}{N} \sum_{i=1}^{N} y_i^4 \right\} \frac{1}{R_q^4} = 2.2 \qquad (4)$$

where $y_{average}$ is the mean line. For this 3-D rough surface, eight slices were cut as shown in Figs. 4 and 5. Figure 4 shows in detail the 2-D slice with the largest R_a (average roughness) and R_q (rms roughness). This slice is denoted as slice 1 in Fig. 5. Slice 8 in Fig. 5 has roughness statistics most similar to the 3-D rough surface. The statistics of all eight 2-D rough surfaces are summarized in Table 1. Each of these rough surfaces were attached to the inviscid/viscous flat plate so that the elevation of the flat plate corresponds to the mean line of the rough surface.

For the 2-D rough surface shown in Fig. 4, six different lengths of the viscous flat plate (L = 0.1, 0.2, 0.5, 1, 2, and 3 m) were examined to understand the effects of the approaching boundary-layer height. For the remaining seven rough surfaces shown in Fig. 5, L was set at 1 m to examine the effects of roughness statistics on the predicted flow and heat transfer.

Table 1. Statistics of 2-D Rough Surfaces

2-D Rough Surface	1	2	3	4	5	6	7	8
R_a (mm)	1.480	1.431	1.108	1.012	0.943	0.881	0.748	1.196
R_q (mm)	1.709	1.637	1.352	1.267	1.133	1.136	0.991	1.407
R_{sk}	0.341	0.312	-0.441	-0.667	0.356	-1.509	-0.317	-0.203
K_u	1.927	1.891	2.229	2.471	3.038	2.589	3.136	2.042

3. FORMULATION AND NUMERICAL METHOD OF SOLUTION

The 2-D rough surface problem described in the previous section is modeled by the ensemble-averaged conservation equations of mass (continuity), momentum (full Navier-Stokes), and energy for air, but the air is assumed to be incompressible with properties at 300K and 1 atm. The effects of turbulence was modeled by the two-equation realizable k-ε model.[21]

Solutions to the conservation equations and the realizable k-ε model were obtained by using Version 6.1.22 of the Fluent-UNS code.[22] Fluent-UNS generates solutions by using the SIMPLE and the SIMPLEC algorithms for problems with steady states. Since SIMPLE is more stable for problems with complicated flow features, SIMPLE was used. All equations (conservation and turbulent transport) are integrated over each cell of the grid system. The fluxes at the cell faces are interpolated by using second-order upwind differencing. In all cases, computations were carried out until the residual plateau to ensure convergence to steady-state has been reached. At convergence, the normalized residuals were always less than 10^{-4} for continuity, less than 10^{-7} for u (x-velocity), energy, k, and ε, and less than 10^{-8} for v (y-velocity).

4. GRID SENSITIVITY AND VALIDATION

Accuracy of CFD solutions is strongly dependent upon the grid system, which must be constructed to minimize grid-induced errors and to resolve the relevant flow physics. To illustrate the procedure employed in this study to generate grid independent solution, consider the simulation of the rough surface shown in Fig. 4 (surface 1 in Table 1). Figure 6 shows the "final" grid system employed, which satisfies the following conditions: the y+ of the first cell next to the wall is less than unity (in fact, less 0.3) and there are at least five cells within a y+ of two (not the typical five). This grid system (grid 3) was arrived at after generating solutions on the following four grid systems: grid 1 (40,426 cells), grid 2 (78,880 cells), grid 3 (98,600), and grid 4 (177,480 cells). The result of this grid sensitivity study is shown in Fig. 7 for the predicted local friction coefficient. In Fig. 7, only the contribution from shear to the friction coefficient is given (i.e., pressure contributions on the rough part of the surface are not included). From this figure, it can be seen that grid 3 yields grid-independent solution. Every solution presented in this paper is made grid independent in the manner just described.

With grid independence addressed, the next issue is meaningfulness of the computed solutions. Since experimental data exist for turbulent boundary-layer flow over a flat plate, computations were performed for the flat plate problem. The results of this validation study are shown in Fig. 8. From this figure, it can be seen that the Fluent computations based on the realizable k-ε model compare reasonably well with the experimental data. Predictions made by other investigators using other turbulence models are also included in Fig. 8.

5. RESULTS

As noted in the Introduction, the objective of this study is to assess the usefulness of 2-D CFD simulations that resolve 2-D slices of 3-D rough surfaces in understanding and predicting 3-D rough surfaces. In this section, the results of the 2-D CFD simulations are presented and – when possible – compared with experimental data to make the assessment.

Effects of Approaching Boundary-Layer Thickness

For the 2-D rough surface shown in Fig. 4 (surface 1 in Table 1), results were obtained for six different lengths of the viscous flat plate upstream of the rough surface to understand the effects of the approaching boundary-layer thickness on flow and heat transfer. The six lengths investigated are L = 0.1, 0.2, 0.5, 1, 2, and 3 m, and they would produce the following boundary-layer thicknesses at the end of that length if the plate continued to be flat beyond it: 0.4366, 0.8691, 1.5374, 2.163, 3.408, and 4.2768 cm. These boundary-layer thicknesses were the ones predicted by Fluent, assuming that the boundary-layer is turbulent from the leading edge of the viscous flat plate. For this 2-D roughness, the average roughness height or R_a is 1.48 mm. Thus, the ratios of the approaching boundary-layer thickness to R_a corresponding to the six lengths are 2.95, 5.88, 10.4, 14.6, 23.0, and 28.9, respectively.

Figure 9 shows the predictions for the local friction coefficient due to shear (C_{ff}), the local friction coefficient due to pressure (C_{fp}), and the local friction coefficient that considers both shear and pressure (C_f). From this figure, the following observations can be made. First, C_{ff} can be positive or negative (i.e., shear can add or reduce net drag of the rough surface). This is because recirculating flows between roughness peaks can cause negative shear. Second, the pressure contribution to C_f is much higher than those due to shear (about one order of magnitude higher) even when gage pressure is used. In fact, the C_f and C_{fp} curves are very similar. Third, C_{fp} is highest at high positive slopes of the roughness that represent stagnation regions. Thus, it is important to understand how geometry affects impingement of the freestream flow on the roughness. Fourth, zeros of C_{ff} represent separation and reattachments points. Fifth, though Fig. 9 only showed a small section of the surface 1, it is fairly representative of what takes place.

At this point, it is important to note that C_{fp} plotted in Fig. 9 is defined by using the gage pressure. Thus, though one would expect the zeros in C_{fp} to be where pressure changes sign about peaks and valleys, this is not the case because gage pressure is used. Thus, if the gage pressure

is below 1 atm, then C_{fp} could be negative even though the slope of the rough surface is positive. Similarly, if the gage pressure is below 1 atm and the roughness slope is negative, C_{fp} could be positive. This confusion could be removed if the absolute pressure is used. Since C_{fp} only has meaning after it has been integrated along the rough surface to yield the net pressure force, less attention should be made to it before it is integrated.

Figure 10 shows the average friction coefficient for the entire rough surface from x = 0 to x = L_r in Fig. 2 as a function of L or the approaching boundary-layer thickness. From this figure, C_f is very sensitive to L when L is small (e.g., L < 1 m). When L gets larger, its effects on C_f diminish.

Figure 11 shows the average St number for the entire rough surface as a function of L. Unlike C_f, St was found to be a strong function of L even when L = 3m.

Figures 12 and 13 show the details of the flow about a portion of rough surface 1. From these figures, one can see where pressure is highest (e.g., stagnation regions) and where pressure is low and shear force may be low and negative because of separated flows.

Effects of Roughness Statistics

For all eight rough surfaces shown in Fig. 5 whose statistics are summarized in Table 1, the approaching boundary-layer was the same (L = 1 m). Figure 14 shows the predictions for the local friction coefficient due to shear (C_{ff}), the local friction coefficient due to pressure (C_{fp}), and the local friction coefficient that considers both shear and pressure (C_f). Figures 15 and 16 show the average friction coefficient and the average Stanton number for the eight surfaces along with the experimental data from Bons, et al.[8]

From Fig. 15, we note that surface 8, which has roughness statistics most similar to the 3-D rough surface, has a C_f reasonably close to the experimentally measured value (though surface 6 predicts even better). But, before we jump for joy, we note that surfaces 1, 3, and 7 all have similar C_f values, but they differ greatly in R_a, R_q, R_{sk}, and K_u. Surface 1 has the highest R_a and R_q values, and surface 7 has the lowest. On R_{sk}, surface 1 has a positive value, whereas surfaces 3 and 7 have negative values. Ku also varies considerably for these three surfaces. Thus, it must be the unique combination of these parameters or some other statistical parameter not yet discovered. Thus, 2-D CFD simulations might be useful as a way to discover the key statistical parameters. From Figs. 15 and 16, it can be seen that values of C_f differ greatly among the surfaces, but the values of the Stanton number are about the same except those for surfaces 5 and 8.

6. SUMMARY

CFD simulations were performed to understand the effects of 2-D roughness on flow and heat transfer.

Results obtained show the complexity of the flow features. In particular, it shows how features of the flow increase or decrease friction coefficient via shear or pressure and how those flow features affect surface heat transfer. The results also shows that traditional statistical measures of roughness – R_a, R_q, R_{sk}, and K_u – do not correlate to friction coefficient or Stanton number. Thus, 2-D simulations of roughness is quite useful as a means to understand the effects of geometry on flow and heat transfer and in providing insight to develop engineering models to predict friction and heat transfer coefficients as a function of geometry.

NOMENCLATURE

c_{ff} local friction coefficient due to shear

c_{fp} local friction coefficient due to pressure based on gage pressure

c_f local friction coefficient that account for both shear and pressure ($c_f = c_{ff} + c_{fp}$)

C_f average friction coefficient due to shear and pressure for entire rough surface (x = 0 to x = L_r)

C_p constant pressure specific heat

St   Stanton number ($q_w'' / \rho U_\infty C_p (T_w - T_\infty)$)

T, T_w, T_∞ temperature, wall T, freestream T

U_∞ freestream velocity

u_τ friction velocity

x-y   Cartesian coordinate system defined in Figs. 2

y^+ normalized distance normal to surface ($\rho u_\tau y / \mu$)

μ dynamic viscosity

ρ density

REFERENCES

1. Taylor, R. P., "Surface Roughness Measurements on Gas Turbine Blades," *ASME Journal of Turbomachinery*, Vol. 112, 1990, pp. 175-180.
2. Tarada, F. and Suzuki, M., "External Heat Transfer Enhancement to Turbine Blading due to Surface Roughness," ASME Paper 93-GT-74, 1993.
3. Bons, J., Taylor, R.P., McClain, S.T., and Rivir, R.B., "The Many Faces of Turbine Surface Roughness," ASME Journal of Turbomachinery, Vol. 123, October 2001, pp. 739-748.
4. Blair, M.F., "An Experimental Study of Heat Transfer in a Large-Scale Turbine Rotor Passage," *ASME*

Journal of Turbomachinery, Vol. 116, 1994, pp. 1-13.

5. Hoffs, A., Drost, U., and Bolcs, A., "Heat Transfer Measurements on a Turbine Airfoil at Various Reynolds Numbers and Turbulence Intensities Including Effects of Surface Roughness," ASME paper 96-GT-169, 1996.

6. Bogard, D.G., Schmidt, D.L., and Tabbita, M., "Characterization and Laboratory Simulation of Turbine Airfoil Surface Roughness and Associated Heat Transfer," *ASME Journal of Turbomachinery*, Vol. 120, 1998, pp. 337-342.

7. Abuaf, N., Bunker, R.S., and Lee, C.P., "Effects of Surface Roughness on Heat Transfer and Aerodynamic Performance of Turbine Airfoils," *ASME Journal of Turbomachinery*, Vol. 120, 1998, pp. 522-529.

8. Bons, J.P. and McClain, S.T., "The Effects of Real Turbine Roughness with Pressure Gradient on Heat Transfer," *ASME Journal of Turbomachinery*, Vol. 126, July 2004, pp. 385-394.

9. Prandtl, L. and Schlichting,H., "Das Wilderstand Gesetz Rauher Platten," *Werft-Reederei-Hafen, 1-4, 1934*.

10. Schlichting, H., "Experimentelle Untersuchungen Zum Rauhigkeits-Problem," Ingenieur-Archiv., VII, No. 1, 1936, pp. 1-34. (Also "Experimental Investigation of the Problem of Surface Roughness," NACA TM 823, 1936).

11. Nikuradse, J., "Strömungsgesetzen Rauhen Rohren," Forsch. Arb. Ing. Wes, 161, 1933. (Also, "Law of Flow in Rough Pipes," NACA TM 1292, 1933).

12. Coleman, H.W., Hodge, B.K., and Taylor, R.P., "A Re-Evaluation of Schlichting's Surface Roughness Experiment," *ASME Journal of Fluids Engineering*, Vol. 106, March 1984, pp. 60-65.

13. Sigal, A. and Danberg, J.E., "New Correlation of Roughness Density Effect on the Turbulent Boundary Layer," *AIAA Journal*, Vol. 28, No. 3, 1990, pp. 554-556.

14. Boyle, R.J., "Prediction of Surface Roughness and Incidence Effects on Turbine Performance," *ASME Journal of Turbomachinery*, Vol. 116, 1994, pp. 745-751.

15. Guo, S.M., Jones, T.V., Lock, G.D., and Dancer, S.N., "Computational Prediction of Heat Transfer to Gas Turbine Nozzle Guide Vanes with Roughened Surfaces," *ASME Journal of Turbomachinery*, Vol. 120, 1998, pp. 343-350.

16. Bons, J.P., "St and c_f Augmentation for Real Turbine Roughness with Elevated Freestream Turbulence," *ASMe Journal of Turbomachinery*, Vol. 124, October 2002, pp. 632-644.

17. Bergstrom, D.J., Akinlade, O.G., and Tachie, M.F., "Skin Friction Correlation for Smooth and Rough Wall Turbulent Boundary Layers," *ASME Jpurnal of Fluids Engineering*, Vol. 127, November 2005, pp. 1146-1153.

18. Bons, J., "A Critical Assessment of Reynolds Analogy for Turbulent Flows," *ASME Journal of Heat Transfer*, Vol. 127, May 2005, 2005.

19. McClain, S.T., Hodge, B.K., and Bons, J.P., "Predicting Skin Friction and Heat Transfer for Turbulent Flow Over Real Gas Turbine Surfaces Roughness Using the Discrete Element Method," *ASME Journal of Turbomachinery*, Vol./ 126, April 2006, pp. 259-267.

20. Wang, Z.J., Chi, X., Shih, T.I-P., and Bons, J., "Direct Simulation of Surface Roughness Effects with RANS and DES Approaches on Viscous Adaptive Cartesian Grids," AIAA Paper 2004-2420, Fluid Dynamics Conference, Portland, Oregon, July 2004.

21. Shih, T.-H., Liou, W., Shabbir, A., and Zhu, J., "A New k-ε Eddy-Viscosity Model for High Reynolds Number Turbulent Flows – Model Development and Validation," *Computers and Fluids*, Vol. 24, No. 3, 1995, pp. 227-238.
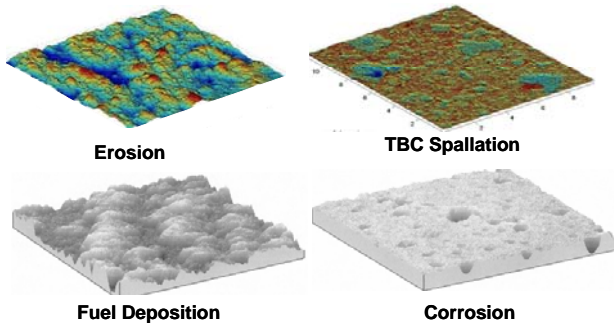
22. http://www.fluent.com/software/fluent/index.htm

Fig. 1. Examples of rough surfaces in gas turbines and their causes (from Bons, et al.[3]).
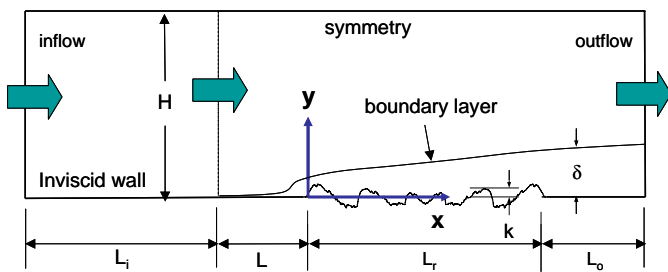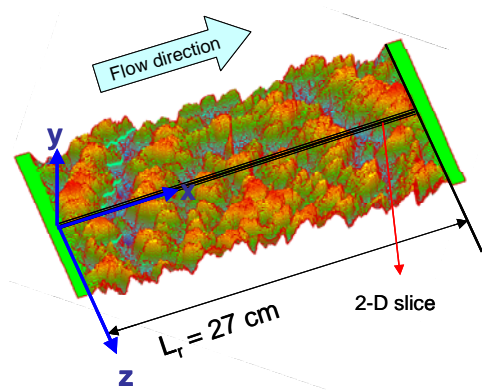

Fig. 2. Schematic of 2-D rough-surface problem studied.

Fig. 3. 3-D rough surface and location of a 2-D slice (Bons, et al.[3]). R_a = 1.17 mm, R_q = 1.44 mm, R_{sk} = 0.11, K_u = 2.2
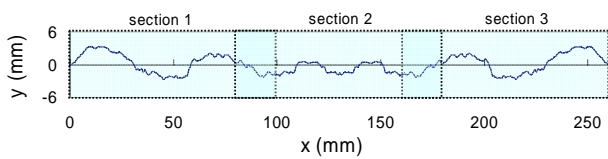

Fig. 4. 2-D slice from 3-D rough surface with the highest R_q, used to study different approaching boundary-layer thicknesses. R_a = 1.480 mm, R_q = 1.709 mm, R_{sk} = 0.341, K_u = 1.928
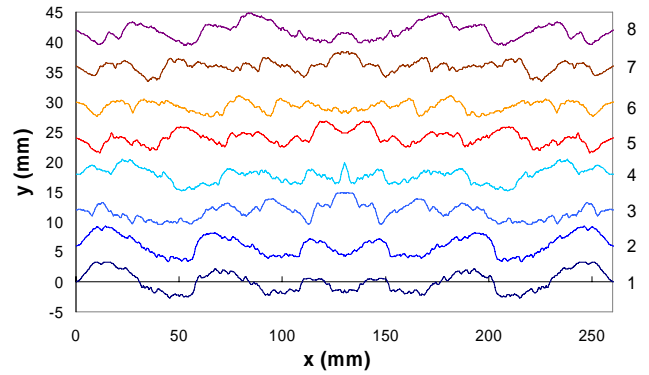

Fig. 5. The seven 2-D slices with the same approaching boundary-layer thickness.
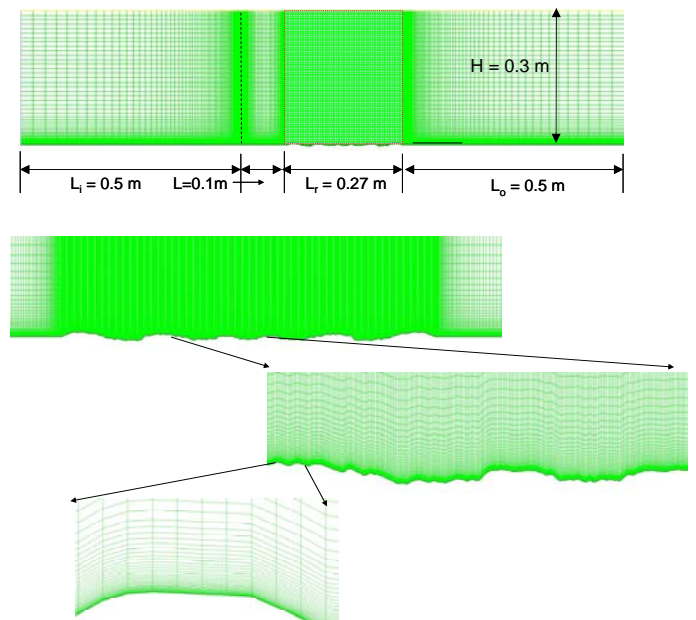
Fig. 6. Example of grid system used. Top: overview. Bottom: zoomed.
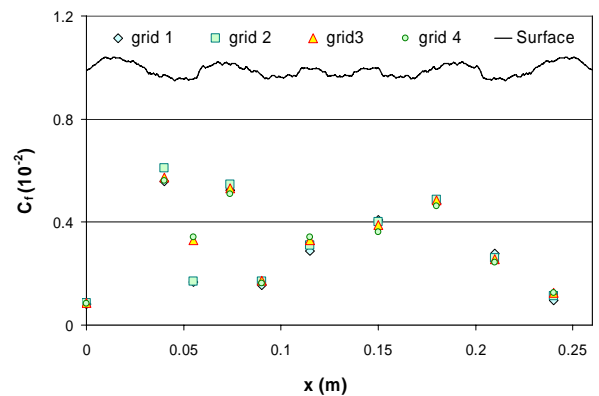
Fig. 7. Grid sensitivity study.
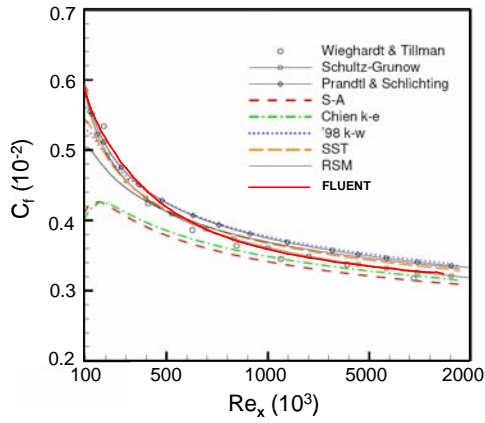
Fig. 8. Validation results for smooth plate (no roughness). Fluent denotes current study.
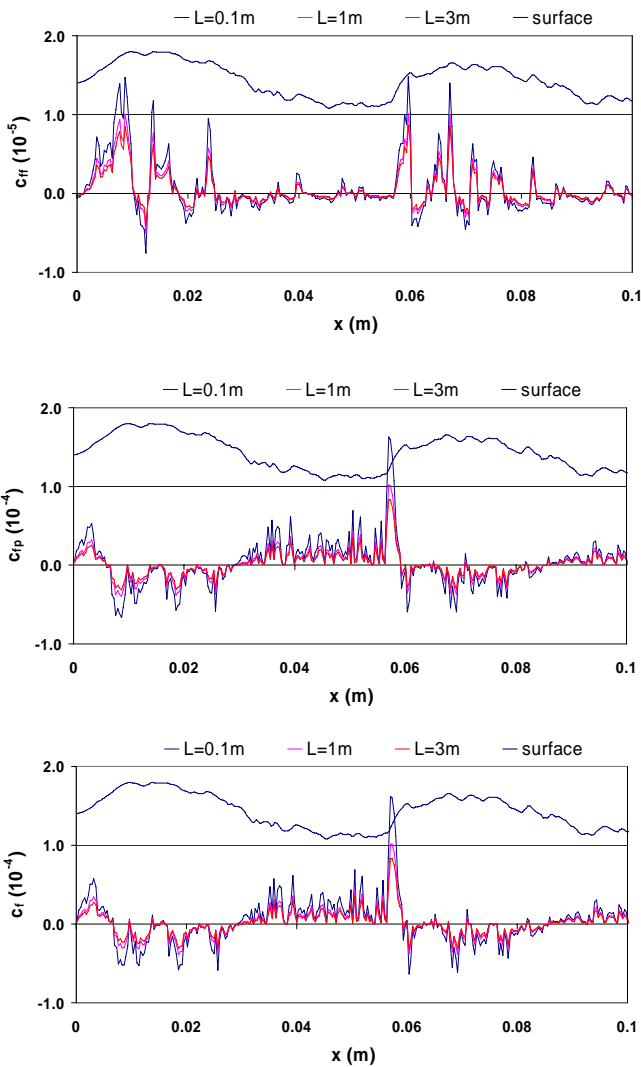
Fig. 9. Local friction coefficient due to shear (c_{ff}), due to pressure (c_{fp}), and due to shear and pressure (c_f) for the 2-D rough surface shown in Figs. 2 and 4 with L = 0.1, 1, and 3 m.
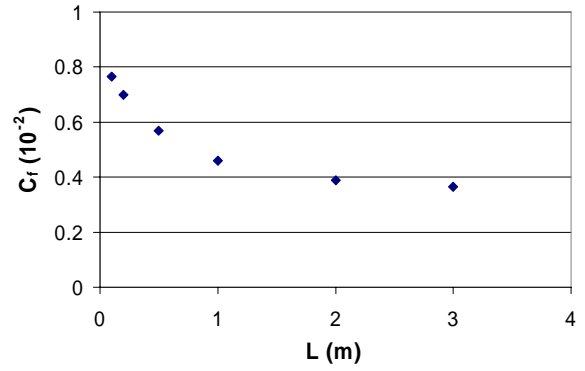
Fig. 10. Average friction coefficient (C_f) for the 2-D rough surface shown in Figs. 2 and 4 with L = 0.1, 0.2, 0.5, 1, 2, and 3 m.
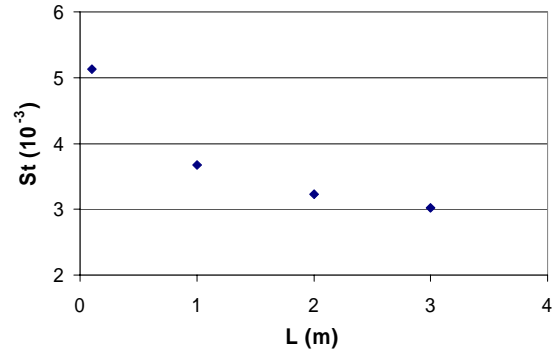

Fig. 11. Average Stanton number (St) for the 2-D rough surface shown in Figs. 2 and 4 with L = 0.1, 1, 2, and 3 m.
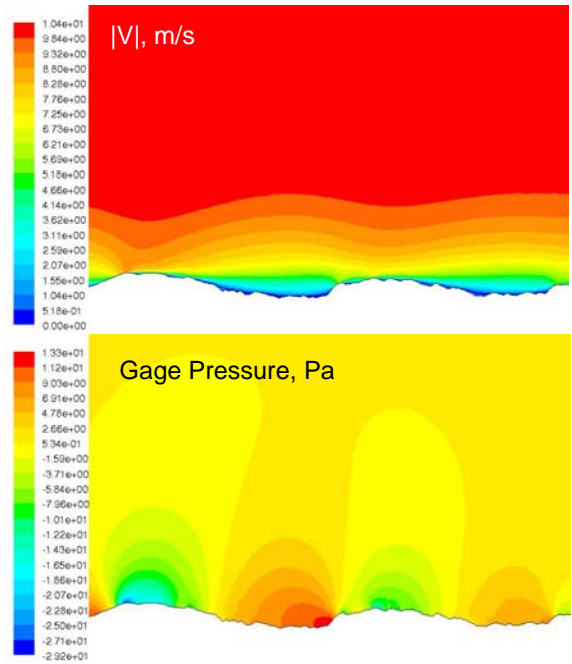
Fig. 12. Contours of velocity magnitude (|V|) and gage pressure (P) for the 2-D rough surfaces shown in Figs. 2 and 4 with L = 1 m.
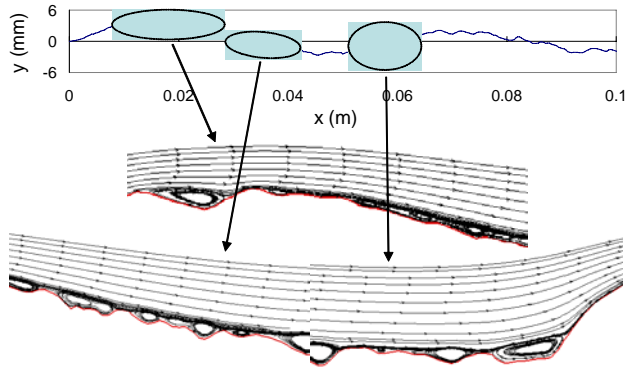
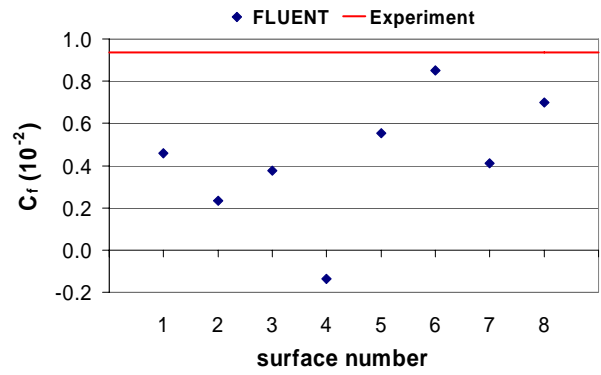Fig. 13. Streamlines for the 2-D rough surfaces shown in Figs. 2 and 4 with L = 1 m.

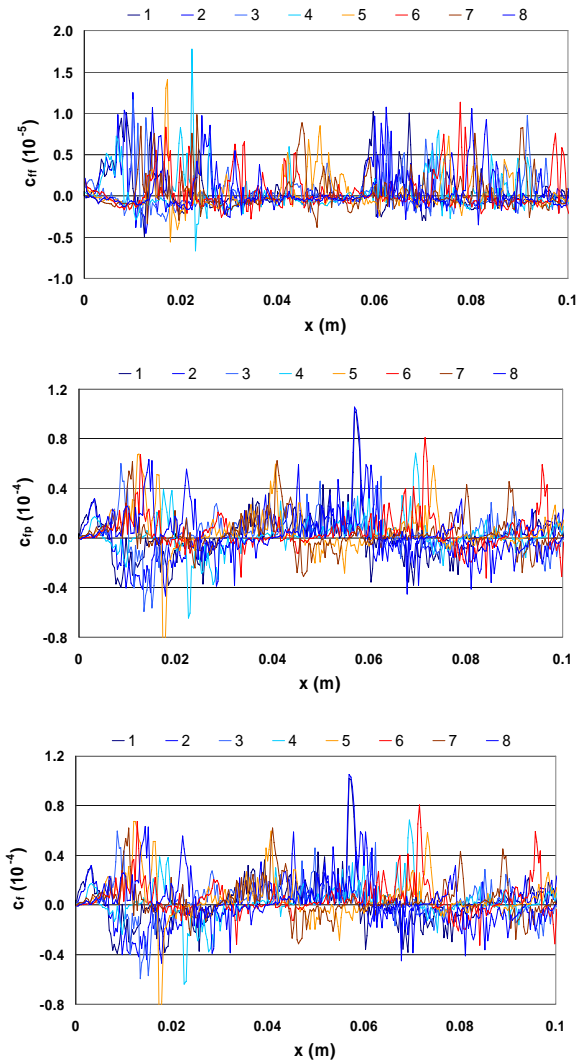Fig. 15. Average friction coefficient (C_f) for the eight 2-D rough surfaces shown in Figs. 2 and 4 with L = 1 m.
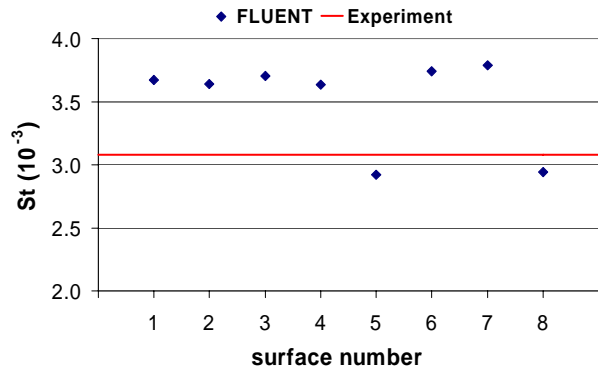

Fig. 16. Average Stanton number (St) for the eight 2-D rough surfaces shown in Figs. 2 and 4 with L = 1 m.

Fig. 14. Local friction coefficient due to shear (c_{ff}), due to pressure (c_{fp}), and due to shear and pressure (c_f) for the eight 2-D rough surfaces shown in Figs. 2 and 5 with L = 1 m.

8